Geotech Geol Eng (2019) 37:1311–1330
https://doi.org/10.1007/s10706-018-0687-4

ORIGINAL PAPER

Predicting Loading–Unloading Pile Static Load Test Curves by Using Artificial Neural Networks

A. K. Alzo'ubi · Farid Ibrahim

Received: 19 June 2017 / Accepted: 28 August 2018 / Published online: 3 September 2018

Abstract In the United Arab Emirates, Continuous Flight Auger piles are the most widely used type of deep foundation. To test the pile behavior, the static load test is routinely conducted in the field by increasing the dead load while monitoring the displacement. Although the test is reliable, it is expensive to conduct. This test is usually conducted in the UAE to verify the pile capacity and displacement as the load increase and decreases in two cycles. The artificial neural network approach was used to build a model that can predict a complete static load pile test. In this paper, it was shown that by incorporating the pile configuration, soil properties, and groundwater table in one artificial neural network model, the static load test can be predicted with confidence. Six thousand field data points were used to train and validate the model. Three complete independent field tests (not included in the training stage) were used to test the model ability to predict the behavior of the pile during loading and unloading cycles. The results show excellent agreement between the actual and predicted curves in two loading–unloading cycles. The authors believe that based on this approach and the presented results of this research, the model is able to predict the entire pile load test results from start to end. The suggested approach is an excellent tool to reduce the cost associated with such expensive tests or to predict pile's performance ahead of the actual test.

Keywords Static load test · Continuous Flight Auger · Artificial neural network

1 Introduction

Deep foundations, such as Continuous Flight Auger (CFA) piles, are usually used to carry and transfer loads of a superstructure to the bearing ground located at some depth below ground surface. Pile's performance is one of the most problematic areas in Civil Engineering due to the variability in geomaterial properties and a large number of parameters controlling pile's design. In practice, three methods of design are used: full-scale static load test, analytic methods, and dynamic methods (Coduto 2001). This paper, however, is concerned with the static load test which is performed by loading or unloading the pile while monitoring the displacement of the pile. The test load is usually applied incrementally up to 1.5 times the design load for working piles load, or more in rare cases, as required by the structural designer or the geotechnical engineer.

As a result of the economic boom that has been happening in the United Arab Emirates (UAE), the construction industry flourished and a huge number of

A. K. Alzo'ubi (✉) · F. Ibrahim
College of Engineering, Abu Dhabi University, Al Ain, United Arab Emirates
e-mail: abdelkareem@gmail.com; abdel.alzoubi@adu.ac.ae

new projects has to be built as fast and as safe as possible. With this in mind, CFA piles, shown in Fig. 1, were heavily relied upon by engineers. The CFA piles are easy and fast to construct in soft ground such as Silty Sand soils which dominate the upper soil layers in the major cities in the UAE. Performing the static load tests is an essential part of checking CFA piles performance which is required by the building code (The Code Handbook 2013). The parameters affecting this performance are the subsurface conditions, such as the soil strength, and the pile configuration, such as the pile length (Crowther 1988; Das 2016).

In this paper, a model that can predict the complete Static Load test was developed using the Artificial Neural Network approach. Training data were collected from three major cities (Abu Dhabi, Dubai, and Al Ain) which are located in UAE. The geology of the chosen cities is consistent which reduced the variations in the geomaterial parameters. Moreover, in this research, a pile diameter of 500 mm was chosen since 80% of about 100 projects explored have a diameter of 500 mm and lengths between 6 and 15 m. It is to note that out of the 100 pile tests explored only one pile has failed to meet the code. This pile exceeds the limit of the acceptable downward displacement of 1% (of its diameter) by moving 1.1% at three times (not 1.5 times) the design load. As a result, only piles within acceptable limits were selected in this research.

This approach would complement the field test, allow judging new proposed pile design ahead of time and cut the cost of conducting multiple static load test for the same project. In fact, Coduto (2001) pointed out that static load tests are much more expensive than analytic methods, and thus the latter is very attractive. However, the calculated load capacities from the analytical method are not as precise as the field test, therefore, designs based solely on analytic methods must be more conservative and the final pile design is more expensive.

Fig. 1 Piles underneath the future Etisalat center in Abu Dhabi

This paper shows that predicting the entire static load test by means of artificial neural networks can be achieved by training the model on the available data. This hypothesis was tested using three independent full static load tests that were not part of the training data. The results showed excellent agreement through different means of statistical analysis. The model prediction accuracy and precision can be further improved through continuous training using future data.

2 Artificial Neural Networks

A neural network is a machine learning model that is trained by processing a set of data records consisting of input parameters with the known output. A backpropagation multi-layer feed forward neural network (BPN) essentially consists of: an input layer, hidden layers, and an output layer. Each layer, in turn, uses a set of connected input/output units with weights associated with each connection. The model learns a set of weights and bias values so as to be able to predict the correct output of the input records. In this model, input attributes are fed simultaneously to form the input layer. The weighted input is propagated forward and passed to the second layer which is the hidden layer; one or more hidden layers may be defined. The number of hidden layers is purely empirical and depends on the experiment result. The net input I_j of a unit in the hidden layer or the output layer is calculated using the following formula:

$$I_j = \sum w_{ij} O_i + \theta_j$$

where w_{ij} is the weight of the connection between unit i in the previous layer and the current unit j; O_i is the output of unit i in the previous layer; and θ_j is the bias at unit j. The bias acts as an adjustment that changes the activity of the unit which is initially assumed. Each time a unit, in the hidden and output layers, takes its input it applies a function to calculate the output O_j at unit j. The function indicates the activation at that unit

and the sigmoid function may be used. The output O_j at unit j is, therefore, calculated using the following formula:

$$O_j = \frac{1}{1 + e^{-I_j}}$$

The output is calculated for each hidden layer until it reaches the output layer, and in this case, it is the model prediction value. This value is compared to the known output value and the error produced is propagated backward by adjusting the weights and biases at each unit to reflect the error in the network prediction. The model will iterate forward and backward on the values assigned to the weights and biases until it reaches an acceptable predicted output value that is within an acceptable error tolerance. Once the model is trained, it can be used to process new input records whose output is unknown. The neural network uses the trained values of the weights and biases to predict the unknown output (Han and Kamber 2012).

3 Related Works

The use of artificial neural networks in predicting the pile capacity started in the 1990's when Goh (1995) used a form of a model to predict an estimate of the friction capacity of driven piles in clay soils. The results were promising when compared to the actual data and some empirical methods. Lee and Lee (1996) tried to predict the driven pile capacity by using an artificial neural network model. The error between the predicted and the actual pile test was around 20%. However, they did not attempt to predict the entire static load test. Abu Kiefa (1998) developed three artificial neural network models to forecast driven piles capacity. He compared the results with four empirical formulas and found that the model that was devoted to forecasting the total pile capacity was more accurate than others with 0.95 coefficients of determination. Furthermore, Goh (1996) presented a new neural network model to predict pile capacity in sandy soils. The output of the model was satisfactory when compared to other empirical formulas.

Shahin et al. (2001) discussed different applications of the artificial neural network in Geotechnical Engineering and mentioned different applications including predicting the pile capacity. Benali and Nechnech (2011) also used artificial neural network to determine the pile capacity; they used a database of 80 cases collected from the literature that expanded different sites distributed all over the world. They reported that the model is feasible for these kinds of problems but they did not attempt to predict the entire static load test. More recently, Maizir and Kassim (2013) used artificial neural networks for predicting the axial capacity of a driven pile; the data collected for this study consisted of 300 cases from several projects in Indonesia and Malaysia. They found that a good prediction was achieved if "both stress wave data and properties of both driven pile and driving system are considered in the input data".

In another experiment (Tarawneh 2013), the pile setup was predicted using an artificial neural network model. The predicted values were compared with those produced by some empirical formulas. It showed that the model produced satisfactory results. A recent paper (Alzo'ubi et al. 2015) proposed a framework for a system model that combines the neural network technique to predict the pile capacity with the containing the pile load tests.

As seen in the above-mentioned studies, no serious attempt was made to predict the entire static load test. In this paper, it will be demonstrated that the static load test can be reasonably predicted by an artificial neural network with enough training data.

4 Subsurface Conditions and Collection of Data

As indicated earlier, the subsurface conditions at which the pile is located plays an important role in controlling its behavior. The subsurface conditions are highly affected by the geological formation of UAE which is situated on the floor of the Arabian Gulf and is mainly composed of extensive carbonate sediments subjected to weathering. Fookes and Knill (1969) divided the mountain and piedmont plain of the Arabian Gulf into four sediment depositions. The coastline of UAE, where this study is performed, is located in zone number four or the base plain. The upper layer deposits of this zone consist of sand dunes, loess, and evaporate together with marine sand and silts. Wind and evaporation, due to the high temperature, are the principal transporting agents in this region.

Although wind-blown material tends to predominate, as great quantities of silt and sand are moved

during periods of high wind, water also plays an important role in this movement and later deposition of high quantities of Silty Sand material. The depth of the Silty Sand layer ranges from 3 to 10 m and it has a major role in establishing the pile capacity due to friction. Flash floods, the last one was witnessed in 2015, are relatively rare, and any water stream actually reaching zone four is usually short-lived after the rainstorm. However, the groundwater table is very high and it can be as close as 0.5 m from the ground surface. This groundwater table can dominate the desert processes by limiting the wind erosion to soils above it; wind erosion more or less stops when sand and silts are damp. Moreover, as the groundwater table is high and evaporation occurs at high rates, capillary pressure also forces water movement from the groundwater table to surface.

In these conditions, a thick salt crust can build and it might also affect the pile's performance. These deposits are common in the urban areas of UAE desert coastal regions and particularly extensive around this coastline. Beneath the first layers of sand and silt, other soil and rock materials exist. The Sand and Silt deposits cover interbedded sandstones, conglomerates, calcisiltite, limestone, and siltstones; clay deposits may also be encountered.

Data from five hundred and sixty one boreholes; collected from different projects in Abu Dhabi, Al Ain, and Dubai, were used in this research. Static pile load tests were then associated with the closest borehole in the same site. Undisturbed and disturbed split spoon samples were obtained from the boreholes. Sieve analysis and the Atterberg Limits test were performed to classify the soil according to the Unified Soil Classification System and later considered as a parameter in the Neural Network input data. In this research, the soil layers were categorized into seventeen different layers and then coded as shown in Table 1.

Friction between the geomaterial and the pile circumference area is an important factor that controls the pile performance. Consequently, the friction angle ($\emptyset'$) of the soil needs to be determined or estimated in order to be incorporated in the neural network. This value was obtained from laboratory test or calculated using the Standard Penetration Test (SPT) that was performed at every one meter of depth in accordance with the ASTM D 1586 (ASTM 2011). The SPT is considered reliable when performed in a granular material such as those encountered in all of the projects in this research.

The SPT (N) values were used to calculate the friction angle (if not measured) such that, the raw N values were first corrected to 60% energy (N60) to compensate for variation in the test procedures according to (Skempton 1986):

$$N_{60} = \frac{E_m C_B C_s C_R N}{0.6}$$

where E_m is the hammer efficiency, C_B is the diameter of the borehole, C_s is the sampler correction, C_R is a correction for the rod length.

Liao and Whitman (1985) suggested that for granular material, the N_{60} need to be further adjusted to take into consideration the effect of the overburden pressure. So the $(N1)_{60}$ calculated from the previous step was modified by using:

$$(N_1)_{60} = N_{60}\sqrt{\frac{100kPa}{\sigma'_z}}$$

where σ'_z is the effective vertical stress at the SPT test location. The effective vertical stress was calculated based on the unit weight of the material at the corresponding depth.

To calculate the effective friction angle of soil, for soils that were not tested in the lab, the following formula that was suggested by Hatanaka and Uchida (1996) was used:

$$\emptyset' = \sqrt{20(N_1)_{60}} + 20$$

Another important parameter that controls the pile's performance is its end bearing. All the piles in this research have reached the rock formation. Consequently, the Unconfined Compressing Strength (UCS) was used as a parameter in the neural network. Samples of the rock layers were obtained using a double tube core barrel of 76 mm inside diameter and tested under uniaxial loading to determine the UCS value.

5 Static Load Test

The pile load tests are considered the most satisfactory method to assess the pile performance. During the

Table 1 Soil description and the soil profile codes used in the neural network model

Soil description	Soil profile	Code
Silty SAND (SM): Dry to moist, light brown, fine non-plastic, trace fine gravel	1	10000000000000000
Poorly graded SAND with silt (SP-SM): Wet, light brown, fine, and non-plastic	2	01000000000000000
MUDSTONE: Very weak to weak, moderately to highly fractured, moderately weathered	3	00100000000000000
MUDSTONE: Weak moderately fractured, moderately weathered	4	00010000000000000
Crystalline Gypsum: Moderately weak moderately fractured, moderately weathered	5	00001000000000000
Loose to medium dense SAND with trace silt	6	00000100000000000
Very loose light brown clayey fine SAND	7	00000010000000000
Dense, light brown fine silty SAND	8	00000001000000000
Weak, slightly conglomeratic CALCISILTITE, distinctly weathered (C), fracture close spaced	9	00000000100000000
weak brown Sandstone mixed with Gypsum	10	00000000010000000
Medium dense to dense becoming very dense, gravely SAND	11	00000000001000000
Very dense, gray, very silty, fine to medium grained SAND	12	00000000000100000
fine-grained, carbonate SAND with some amount of gravels	13	00000000000010000
Weak, slightly-moderately weathered, CALCARNITE	14	00000000000001000
Very weak, light brown, poorly to well cemented calcareous SANDSTONE	15	00000000000000100
Medium dense, dry to moist, non-plastic, poorly graded SAND (SP)	16	00000000000000010
Very stiff, light grey, wet, non-plastic, sandy SILT (ML) with a trace of shells	17	00000000000000001

foundation construction period, it is recommended that such tests be performed according to British Standard Code of Practice 8004 on specially constructed piles that are installed before the start of the general construction works. Figure 2, shows the static load test performed in the future Etisalat center (see Fig. 1). In the static pile load tests, the load–displacement curves were obtained through two cycles of loading–unloading.

Fig. 2 Static load test in the future Etisalat center

The common practice in the UAE (The Code Handbook 2013) is to test the piles after construction for quality assurance and not for design; i.e. to check performance. As a result of this practice CFA piles, in most cases, are over-designed to avoid failure in the testing process. However, if testing is carried out for design purposes, significant savings may result from a more economical pile design based upon the specific test data. The proposed method in this research would enable designers to avoid over designing the piles through studying the predicted static load test curves produced by the neural network prior to conducting the field test and revise their design. Note that the theoretical design methods provide only an approximate working load, while the static load test should demonstrate the pile's performance and its load settlement characteristics.

In order to have a satisfactory design, Tomlinson and Woodward (2014) established that for full skin friction mobilization, the pile needs to settle at least 1% of its diameter. While to mobilize the full end-bearing capacity, settlement of about 10% of its diameter is needed. Terzaghi (1943) and Meyerhof (1965) specified that the maximum vertical movement of a pile should not exceed 25 mm, no pile in this

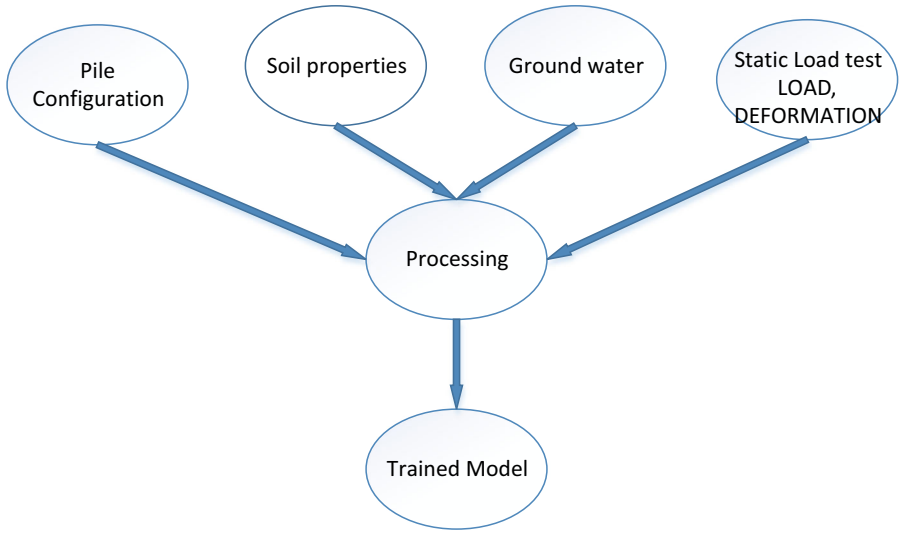

Fig. 3 Training cycle in the artificial neural network used in this research

paper got even close to this value (the maximum measured total settlement was 4.0 mm). Also according to the above discussion, a very small portion of the end-bearing resistance was mobilized if any. In addition, the maximum allowed residual settlement is 6 mm, this is to avoid pile failure for piles under 600 mm in diameter (Das 2016), no pile in this research has experienced this amount of residual settlement.

In this research, the load was applied in increments up to 1.5 times the design load for working piles load. The load was applied by means of a hydraulic jack as shown in Fig. 2, four reaction piles were used to provide support for the loading frame. In addition, four settlement gauges were used to monitor the displacement. The maintained load method was used in all of the projects; the load was increased in stages and maintained for at least 20 min or until the rate of settlement decreased to less than 0.10 mm/hr, whichever is greater. As a matter of fact, in all of the projects, the load was maintained until the settlement has seized. In the first loading cycle, increments of 25% of the design load; up to the working load, are imposed on the tested pile and maintained until settlement seized. Settlement readings were taken, for each load increment, every 5 min until the settlement stopped.

In the first unloading cycle, the load was reduced in the inducement of 25% until the zero load stage is reached while monitoring the displacement. The pile is then reloaded to the test pile from zero to 150% of the design load such that the 100% of the design load is applied and kept for six hours. The load was then increased in 25% (of the design load) increments until the test load was reached. At last cycle, the pile is unloaded in the inducement of 25% until zero loads while monitoring the displacement at each load. The loading/unloading values and their corresponding displacement were input to the neural network in the same sequence as described above.

6 Network Topology and Setting

This research is aiming to build a model in which it is possible to predict the displacement value using an artificial neural network that is trained over data consisting of a combination of the soil profile and the pile configuration, as shown in Fig. 3. Hence, if S_i is assumed to be the set of soil profile values at site i and whose elements consist of values in the set $\{v_1, v_2,\ldots,v_j\}$ and P_i be the set of pile configuration at site i, and whose parameters consists of $\{p_1, p_2\}$, then for an applied load L_j and a groundwater table G_j it is possible to predict the displacement D_j such that $F(S_i, P_i, L_i, G_j) = D_j$, where F is a mapping function for all values of j in the pile test. This mapping function will be built using a trained artificial neural network.

A specialized software (Neural Planner Software 2016) was used to construct the artificial neural network. The model, shown in Fig. 4, consists of 28 input units; each corresponds to an attribute. These attributes are shown in Table 2 along with their range

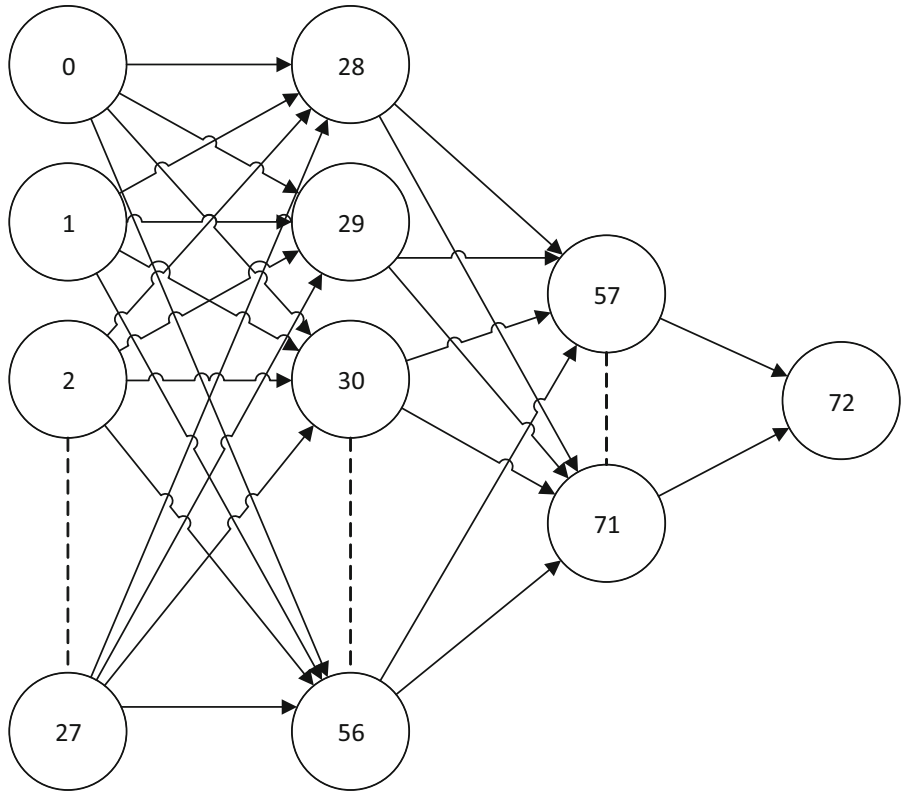

Fig. 4 The artificial neural network configuration used in this paper, two hidden layers are shown

of data. The 28 input units are such that: 17 for the soil profile, 4 for the loading status, 2 for the pile configuration, 1 for the groundwater table, 1 for the load, 1 for the depth, and 2 for the soil properties. Moreover, Tables 1 and 3 show the soil profile and the status attribute values and their codes, respectively. The setting of the hidden layers was empirical where two hidden layers were chosen. There were 29 units in the first hidden layer and 15 units in the second. The initial weight setting was the default value of 0.6, the target training error was set to be 0.01 for all training records. 6437 Pile data points were collected from the field, as described in Sec. 4, such that 5537 points were used for training and 900 random points were selected for validation.

Although the neural network software has different criteria to stop the training, shown in Fig. 5, two of which were used: all training errors are below the target error, or when the validation error starts to increase whichever comes first. The latter is called early stopping (Liu et al. 2008; Prechelt 2012) which is necessary to avoid overtraining and consequently overfitting (Haykin 1999; Liu et al. 2008). The produced model should generalize the mapping between input and output and should be capable of predicting the output for cases not included in the training set (Geman et al. 1992).

With this setting, the training stopped at the epoch of 5701 when the validation error was reported to be increasing. In this software, the average validation error value is considered as increasing when it is found increasing in six successive cycles. The values that were scored before training terminated, were as follows: 0.00088148, 0.00088566, 0.00089362, 0.00089493, 0.00090312, and 0.00090459. The average training error was 0.00053867, while the maximum training error was 0.03651359 as shown in Fig. 6. Moreover, Fig. 7 shows how the predicted output points, scaled between 0 and 1, are distributed near the regression line for both the training and validation examples. The biases and weights that were produced in the model are shown in Tables 4, 5, 6 and 7.

Table 2 Input attributes in the artificial neural network and their data types

Attribute name	Data type	Data name	Values
Pile length (m)	Real number	PileL	6–15 m
Pile diameter (mm)	Real number	PileD	500 mm
Load (ton)	Real number	Load	0–165
Average displacement (mm)	Real number	AverageD	0–3.433
Status (loading–unloading)	Integer value	Status	2 cycles of each (see Table 3)
GWD (m)	Real number	GWD	1.1–5.9 m
Depth (m)	Real number	Depth	0–17 m
PHI (°)	Real number	PHI	27–43
UCS (kg/cm^2)	Real number	UCT	0–52.8
Soil profile (see Table 1)	Integer value	SoilPf	1–17

Table 3 Codes for the loading–unloading cycles used in the training and testing cycles

Status	Code value
First loading	1000
First unloading	0100
Second loading	0010
Second unloading	0001

7 Sensitivity Analysis and Input Importance

As indicated earlier, the displacement of the pile is controlled by the assumed parameters: pile configuration, soil, groundwater table and load. To test the relevance of these parameters to the resulted output a sensitivity analysis has been conducted to show how much an output changes when the inputs are changed during the experiment. After setting the inputs to the median values, the change in the output was measured

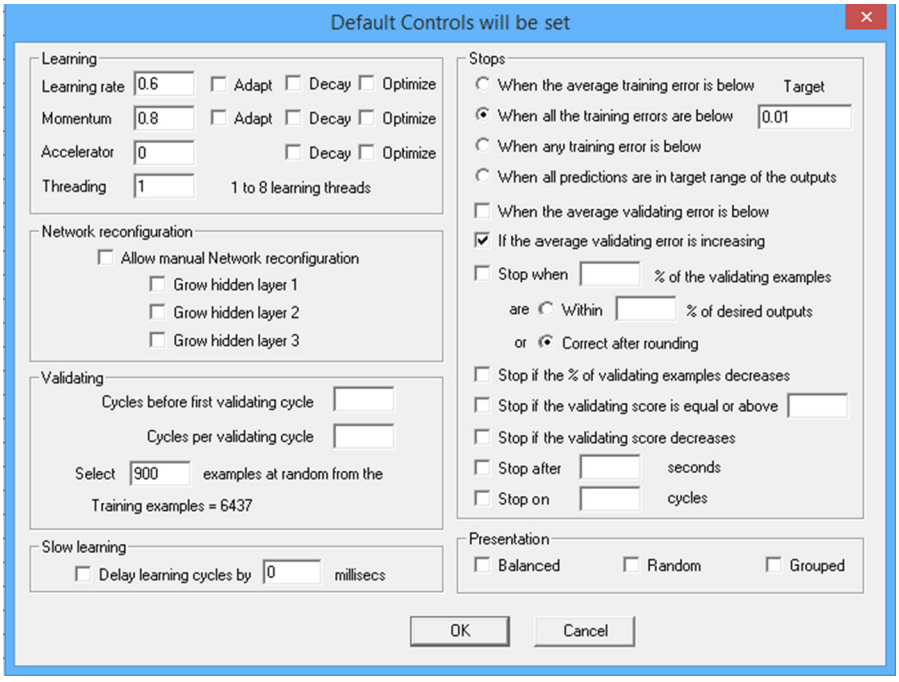

Fig. 5 The artificial neural network setting using the implemented software: EasyNN

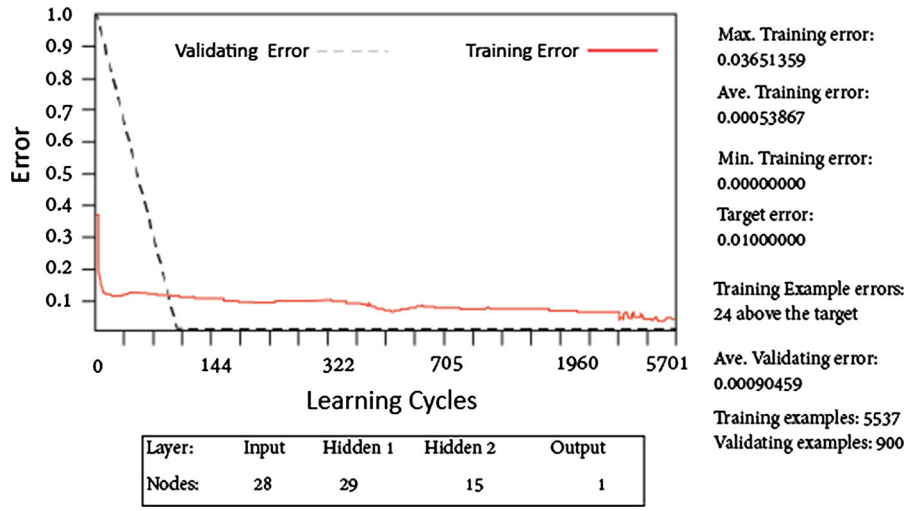

Fig. 6 Training error variation as observed in the artificial neural network model

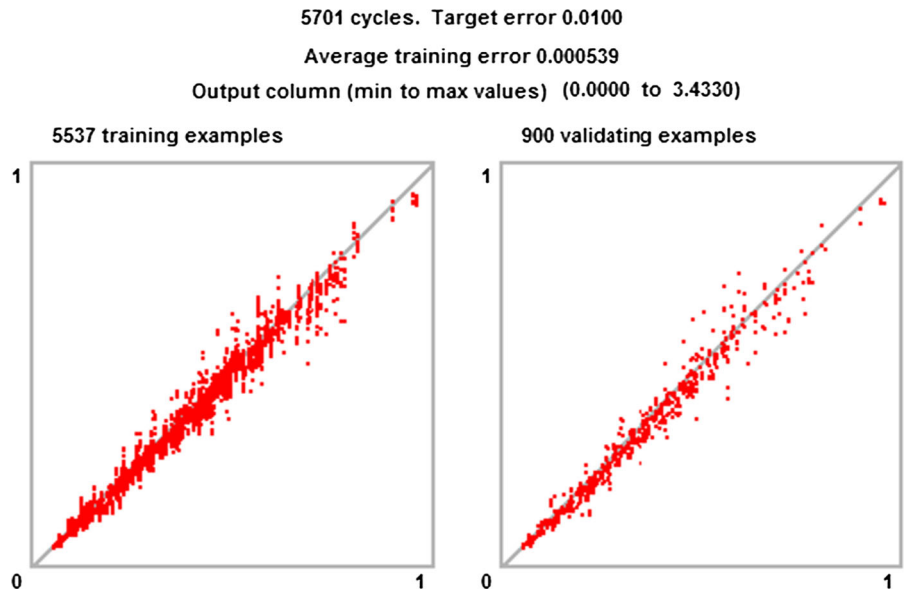

Fig. 7 The prediction process for the training and validation examples produced by the artificial neural network

as each input was increased from the lowest to the highest values to establish the sensitivity of the output to that change. Figure 8 shows the summary of the sensitivity of the input parameters in descending order.

This figure shows that the displacement is sensitive to the variation of all of these input parameters in different degrees. However, the pile diameter is the least significant since the trained data was limited to only one diameter value. The diameter was removed from the input to examine if the model performance improved, however no positive impact was observed. So, the diameter was kept for future extension of the model by adding more pile's diameters to the training data. Moreover, the summary of the importance of the input parameters was also shown in Fig. 9. In this experiment, the importance of each parameter is calculated as the sum of the absolute weights from its input node to all of the nodes in the first hidden layer. The input importance indicates that all the inputs were active and important until the training was terminated except the pile diameter which was limited to one value. In this analysis, the soil profile as well as the loading status was plotted in Fig. 8 as a one parameter to show the sensitivity of the model to the soil type or the loading status as well their importance.

Table 4 The Bias values at each node

Node	0–27	28	29	30	31	32	33	34	35	36	37
Bias	0.0	1.468495	1.452067	− 0.707321	− 5.920155	− 2.306580	− 0.118795	− 2.031410	− 5.085564	− 3.163887	A.197607
Node	38	39	40	41	42	43	44	45	46	47	48
Bias	− 5.113705	− 1.018970	− 2.526465	− 1495257	0.972878	− 1.733526	− 2.498516	41.508031	− 5.551098	− 13.026989	− 0.229659
Node	49	50	51	53	54	55	56	57	58	59	60
Bias	2.190136	2.021920	2.021920	0.049576	− 3.623429	− 8.548299	2.241019	− 4.924333	− 2.303421	− 2.277171	− 7.310964
Node	61	62	63	64	65	66	67	68	69	70	71
Bias	− 9.473724	− 4.008005	− 7.801761	− 2.093086	− 0.197827	− 1.394436	0.214764	− 0.375857	− 1.630187	− 7.911063	− 5.145810
Node	72										
Bias	0.539494										

8 The Test Plan

The test plan was carried out by using three independent field tests from different sites to examine the model accuracy. All of the three piles have 500 mm in diameter, while the length of piles 1, 2, and 3 were 6 m, 7 m, and 8.5 m, respectively. Not only the pile length varies, but the soil profile, friction angle, unconfined compressive strength, and groundwater level were also varying from test to test as shown in Table 8.

A query file is created for each pile test and was individually processed by the artificial neural network. Each row in the file was regarded as an input that was processed to predict the displacement at each load. The load was increased in each successive row in the same sequence as conducted in the field test. In the following discussion the predicted displacement value is termed as "predicted", and the actual displacement value as "actual". Two types of graphs were plotted and discussed for each run:

- Load versus displacement graphs to show the actual and predicted values in the same conventional method used in foundation engineering.
- Predicted versus actual displacement linear regression graphs.

9 Discussion

The test on all piles, in this paper, was executed successfully in terms of compression, stiffness capacity and has resulted in acceptable load-settlement performance. Each pile has been able to sustain a load of 1.5 times the safe working load with a total settlement of less than 1% of pile diameter, as shown in the following discussion.

9.1 Load Versus Displacement

Figures 10, 11 and 12 show the load–displacement curves for query files 1, 2, and 3, respectively. The actual field data were also plotted on the same graph for comparison purposes. As shown in the figures, excellent agreement between the field and the model prediction was achieved.

In Fig. 10, the model predicted a maximum displacement of 2.55 mm which is approximately

Table 5 The weight values for connections between the input layer and the first hidden layer

From node	0	1	2	3	4	5	6	7	8	9	10
To nodes 28–56	− 15.454379	0.081083	− 0.857842	− 0.936445	− 0.129716	1.678700	1.430096	− 50.3213489	11.149310	− 12.234247	3.778227
	− 3.343017	0.327612	− 1.951908	− 1.575240	0.121339	0.657742	1.438433	4.012033	− 4.372360	− 12.358190	1.356406
	0.247170	0.301260	− 1.982656	− 3.085405	0.398690	− 0.221598	0.918925	− 1.872029	− 0.315050	− 0.139254	1.837555
	2.787455	0.320710	6.712177	− 0.530456	− 2.261065	− 0.111214	− 3.387376	− 5.737698	1.718424	0.392207	0.262210
	− 7.131533	− 0.103523	− 2.760890	0.612390	4.526115	− 0.668955	− 1.195560	2.444513	5.531360	0.515223	− 2.331657
	− 6.004088	− 0.351091	− 0.483138	2.628403	− 0.83005	− 1.068502	− 0.900766	− 3.849439	7.676338	− 13.690953	− 2.523181
	− 7.818766	0.109315	1.677769	− 8.686949	3.406140	2.194124	2.232720	15.832437	5.897738	− 12.740581	0.170706
	− 0.855216	0.3943 65	13.367456	− 2.483211	0.483810	− 6.246159	2.378952	0.335309	− 0.545202	− 0.351438	0.536879
	6.602344	0.291187	4.49021	− 2.815852	− 0.158208	− 1.445041	1.316510	− 1.896781	− 1.080328	0.375705	5.618111
	− 6.794450	− 0.341157	8.618479	− 0.828018	− 1.151282	− 2.045007	0.369730	− 17.951535	3.906843	0.040417	− 0.502313
	5.264634	− 0.171228	0.273632	− 1.922418	− 2.120188	− 1.042307	0.309716	7.871999	− 16.850515	6.436824	− 3.433400
	7.475034	0.511162	− 2.635497	1.542478	− 0.816331	− 0.758170	− 0.861227	− 3.448952	0.995694	0.580440	1.734 659
	3.747641	− 0.036955	− 1.513808	2.446439	3.193847	− 4.760650	− 3.708495	0.629008	0.718027	− 1.074090	1.622527
	7.034199	− 0.256063	− 3.162406	− 0.083355	− 1.899264	0.147242	− 2.298251	− 7.994765	− 1.395569	0.239695	− 1.496735
	− 3.339985	0.155145	0.867146	0.524020	0.717307	− 0.710636	− 0.450494	− 30.040825	− 21.341929	11.269126	− 5.227269
	− 3.601599	0.072766	2.487951	− 0.028173	− 0.713280	− 1.343000	0.807278	0.809160	− 6.770600	2.487761	− 1.252707
	− 18.239090	0.421329	0.570945	− 1.304081	− 1.058176	− 1.095390	− 0.869994	31.105956	− 2.155572	1.990095	− 6.500989
	16.997873	0.150644	− 5.007779	− 3.344573	− 3.179305	− 2.301793	− 2.143047	5.568048	− 0.638367	0.021053	− 0.445677
	1.899963	− 0.164857	3.903522	− 0.736520	− 0.415511	− 2.735259	− 1.311126	17.801555	0.353150	0.150330	− 2.963475
	14.091170	0.132507	− 0.899950	− 3.398987	− 3.432980	− 2.918943	− 3.819446	25.828494	0.303923	− 0.059321	1.593221
	− 1.293778	0.432610	− 9.021287	1.601791	− 0.762078	− 0.144231	− 0.444642	1.390534	0.547768	− 0.109293	0.385547
	0.402319	0.20828 1	− 11.318767	− 2.131818	− 1.792454	6.210699	− 0.926309	3.917203	− 3.880525	− 0.100127	1.012144
	9.748474	− 0.23 5151	2.143915	− 0.881073	− 0.649534	− 1.384607	− 0.777751	− 16.405390	− 0.041156	− 0.793343	2.121499
	0.521109	− 0.054143	− 12.702143	− 1.397745	− 0.450609	− 0.235602	4.192563	− 0.696984	0.421243	− 0.276690	0.593538
	0.056220	0.284928	− 3.191969	0.716828	− 0.685907	− 0.188843	− 1.241503	− 0.052890	− 6.142942	1.702214	4.768435
	19.795597	0.033808	2.410496	− 2.236189	− 1.144262	− 1.72165	− 1.253749	7.105807	− 0.351248	− 0.480162	2.474095
	− 5.759415	0.346627	2.074142	− 3.947091	− 2.600950	1.701404	1.026912	0.346307	0.888548	4.146806	1.380909
	8.850733	0.286474	2.655964	− 4.979283	− 1.681601	− 0.410031	− 0.583421	− 8.628961	5.035599	0.347260	3.471154
	− 2.127077	0.451577	− 0.254278	0.043348	0.404133	1.169966	0.995901	− 4.936176	− 9.280947	− 20.655018	− 5.713438

Table 5 continued

From node	11	12	13	14	15	16	17	18	19	20	21
To nodes 28–56	2.118094	− 0.226008	0.662006	− 2.720778	− 0.401109	0.231368	− 0.303586	0.144959	− 1.288185	0.739404	− 0.817615
	− 0.155591	− 0.033269	− 1.376078	7.205142	1.839493	− 1.029951	− 1.991760	− 0.947161	− 0.573528	0.873287	− 1.263521
	− 1.082111	1.256798	− 1.757075	− 1.683681	0.586364	− 1.171937	0.450725	0.882054	0.261455	− 0.234 622	0.363763
	− 0.101621	− 0.012198	− 1.433679	− 0.876226	− 1.915021	− 1.277487	− 0.334415	− 1.475845	− 1.006999	− 0.605234	0.002326
	2.439592	0.157810	− 0.209833	2.789112	− 0.484393	− 0.130639	− 0.199581	0.774227	0.161983	− 0.400895	− 1.447116
	− 1.258500	− 0.939640	1.610717	− 1.256127	− 0.216715	− 1.040872	− 1.220374	− 0.133599	− 2.090995	− 0.888980	0.494301
	− 0.991214	− 0.409976	1.839206	− 2.166945	− 1.000694	− 0.073656	0.945787	− 0.398162	− 1.158372	0.298426	− 2.647549
	0.310480	− 0.020348	0.687765	0.380338	0.101326	− 3.487870	− 0.641745	− 0.001016	0.248764	0.120385	0.374147
	0.595041	1.710562	− 0.173198	− 0.972821	1.419460	− 0.472504	− 0.103455	− 0.316551	1.670926	− 0.756182	− 5.059054
	− 0.897144	0.249438	2.086211	− 4.070700	0.659010	− 0.436009	0.445352	− 0.085232	− 1.131423	− 0.440916	− 1.536697
	− 5.152984	1.633493	0.265237	2.564777	6.619423	− 4.580352	− 0.610931	− 2.885103	− 0.169085	1.153891	− 0.673309
	0.178422	− 0.429723	− 0.333964	− 1.380468	0.170612	− 0.378352	0.777074	− 0.880413	0.011386	0.444902	2.365902
	− 0.336788	− 1.719200	− 0.030953	− 1.320800	2.242276	1.947057	0.432181	0.199060	− 0.520200	− 0.173750	1.556329
	− 0.115389	− 0.587984	0.847 555	1.243842	0.021928	− 5.228717	− 1.010171	− 0.065764	0.204267	0.0973355	− 0.420943
	− 3.041366	0.994354	3.751077	− 1.920260	0.145731	− 0.840168	2.359776	− 1.900780	− 2.169167	− 0.775572	0.465547
	− 5.061414	− 0.0749940	0.467243	1.772219	− 0.079647	1.124819	− 0.083462	1.039946	0.320343	− 0.342821	0.171058
	− 0.323159	0.229226	− 1.301299	− 0.419800	− 0.217472	0.053400	− 0.117133	0.370610	− 0.20914 3	0.202897	− 0.004068
	− 0.179458	0.575870	0.438056	0.263554	1.091740	1.392951	− 0.198734	0.04 52 84	0.235147	0.782443	− 0.670411
	− 0.099255	− 0.978153	0.248947	0.307554	− 0.746286	1.260409	0.231463	0.863845	0.789332	− 0.185442	− 2.746395
	0.000208	0.264716	− 0.445282	− 0.382453	− 0.414781	2.534295	2.028508	1.232041	− 0.427033	− 0.125024	− 1.279749
	0.683546	− 0.286030	0.310495	− 0.221912	− 0.022615	2.993497	− 0.273078	0.237261	0.278519	− 0.194118	− 0.713235
	− 1.632273	1.009785	0.227303	0.140508	0.336595	1.152222	0.569025	0.332473	0.089529	0.300795	3.000993
	1.730275	2.718560	0.744548	0.286575	0.350638	− 1.544529	0.646585	− 1.153721	1.156557	0.541141	− 1.816973
	− 0.061791	0.509512	− 0.053488	− 0.441917	1.658346	0.498846	0.243598	0.561702	0.158901	0.225764	0.371767
	− 3.075693	2.141360	− 0.931119	3.459833	0.801250	− 1.372869	0.192696	− 0.440783	− 0.302977	− 0.423443	0.788406
	− 2.840460	− 0.049730	− 0.324132	− 3.435707	0.142550	− 0.175742	0.005420	− 0.455997	− 3.130162	− 3.116957	4.88935
	0.917139	0.201218	− 0.599803	− 0.465005	− 1.784480	0.109029	0.711406	− 1.066453	1.994953	− 0.602447	0.553586
	0.684693	0.141767	− 2.683906	− 3.292271	− 1.406820	− 5.122719	0.886491	− 1.103792	1.191887	− 0.474931	− 2.036894
	− 5.652238	− 0.475100	0.405356	− 0.782540	0.155987	8.117542	− 2.861950	0.085913	− 3.617772	0.234483	− 0.400149

From node	22	23	24	25	26	27
To nodes 28–56	− 0.021186	− 0.003499	2.027335	0.030093	0.377674	0.396895
	0.098579	− 0.703356	− 2.404045	1.242977	− 0.220111	− 0.301847
	0.568454	− 0.505772	− 2.817860	1.342440	− 0.430678	− 0.895963

Table 5 continued

From node	22	23	24	25	26	27
	0.289685	− 0.192317	− 1.039518	0.103241	0.493139	− 0.189919
	− 1.013713	− 0.527191	− 2.574390	0.203756	0.478587	0.039256
	0.086811	− 0.221960	4.513797	− 0.099998	− 0.234498	0.541054
	− 0.842156	− 0.705569	0.885674	− 0.870037	0.434591	0.871846
	0.825018	0.572028	0.456284	− 0.010280	0.318192	0.951043
	1.539216	0.479377	− 0.313847	− 1.035945	− 0.631888	− 0.783812
	0.645181	0.945159	− 2.505527	− 0.309226	− 0.120492	− 0.808026
	− 1.001151	− 0.344929	8.147755	− 3.132999	− 0.894872	− 1.908936
	1.063872	0.147653	− 3.701561	2.289052	0.026009	0.098305
	1.542397	− 0.178543	1.129005	0.046008	− 0.082857	− 0.339104
	0.007190	0.057200	− 0.154279	0.011209	0.487160	0.154987
	0.034032	− 0.145431	− 0.346625	− 0.050406	0.302765	1.203835
	− 0.425942	0.375454	− 0.277352	− 1.761275	0.311517	− 0.639195
	0.096986	0.066719	1.066301	− 0.530314	0.006679	− 0.851987
	0.213735	0.458672	0.589179	− 1.057495	0.038686	0.023275
	− 0.405978	0.242917	1.744974	− 0.015799	− 0.994138	− 0.351971
	− 1.523118	0.023252	2.654956	0.069561	0.021690	− 0.448234
	− 0.853795	− 0.456841	− 1.204733	0.442814	− 0.178416	− 0.158743
	− 0.301144	0.367751	2.735616	− 0.405801	0.117368	− 0.712475
	0.894673	− 0.118104	2.227281	− 0.509750	− 0.201316	− 0.227087
	− 0.263787	− 0.444881	− 0.825018	− 0.457793	− 1.013490	− 0.290418
	0.105887	0.453723	1.294758	− 0.549235	0.342326	0.533250
	1.932324	1.452824	− 0.551553	− 0.458564	0.074062	− 0.726494
	− 0.660707	− 0.174058	− 3.125167	− 0.878455	− 0.501202	0.394639
	1.001629	− 0.299079	3.985991	2.722687	1.380262	0.888939
	0.013483	0.122315	9.133503	− 0.105995	0.813205	0.545014

Table 6 The weight values for connections between the first and second hidden layers

From node	28	29	30	31	32	33	34	35	36	37	38
To nodes 57–71	2.540740	− 0.399282	0.905437	− 2.248816	− 1.670910	− 3.420938	0.163526	− 0.714531	0.543805	1.819879	3.714496
	− 2.398579	− 1.032007	0.053869	− 1.766372	0.364477	4.335641	− 1.681380	− 0.945217	0.345066	− 2.162068	− 2.560029
	− 0.072777	− 2.627111	− 0.907929	− 1.182258	0.400598	− 2.743595	1.393559	− 0.820253	− 1.298704	− 2.901705	0.925554
	10.930880	− 1.750501	− 1.483299	0.681712	− 0.169371	− 7.594692	− 7.162032	1.013302	− 1.390944	3.838427	− 0.934037
	− 3.762654	− 5.082446	− 0.925138	− 2.475633	− 2.030127	− 1.352865	− 3.128807	− 1.038942	2.300908	0.721725	− 1.987026
	3.100129	− 7.247574	− 0.283971	− 2.713717	2.011587	2.979903	− 7.561115	− 0.243145	− 1.972605	4.439920	− 2.461301
	− 0.584289	− 0.206990	− 0.432630	− 2.085690	0.119611	0.996165	0.209312	− 4.720550	− 2.091928	− 1.176100	0.904062
	0.817652	5.945912	− 1.753001	− 2.573355	− 0.715197	1.046231	− 0.726119	− 0.513359	− 1.053920	− 1.464094	− 2.065080
	− 2.121884	0.033756	− 1.423236	− 1.257272	− 0.351205	3.147515	0.627608	0.537574	− 3.125099	− 4.048344	0.438901
	− 0.554135	0.113886	0.063200	− 0.666453	− 0.176539	− 0.304180	1.292978	0.087978	− 0.513575	− 3.642963	_0.256382
	− 6.052812	− 0.635928	− 0.149309	− 0.539450	1.632819	− 1.569923	− 0.724361	− 0.068677	1.227475	− 2.710711	− 0.783674
	− 1.279300	− 0.431156	− 1.857188	− 0.352955	− 0.996028	1.213861	− 0.241004	− 4.710523	− 1.005458	0.569596	0.343370
	− 3.269852	0.262419	− 0.907115	0.913339	− 5.257517	7.853990	− 0.712572	0.280956	1.929920	0.670161	− 3.129830
	− 0.152836	1.797145	0.844006	− 0.750200	1.108039	− 0.890342	− 5.498438	0.122401	0.370751	0.471393	2.554166
	− 0.637416	− 0.344600	− 2.363264	− 0.313075	1.669467	− 1.618282	0.504326	0.531008	_0.918576	− 0.864114	− 2.730706

From node	39	40	41	42	43	44	45	46	47	48	49
To nodes 57–71	1.125364	4.053822	0.931110	1.365954	− 0.784377	− 0.959977	− 2.205909	2.347455	0.199321	2.380359	0.394717
	0.816636	− 1.895446	1.142443	1.380689	0.403142	0.086268	− 1.899199	0.7611369	− 1.829061	1.493680	0.982839
	− 0.141272	0.682722	0.007829	− 0.972925	1.098686	1.173895	2.037936	− 3.305614	− 0.096703	3.453815	1.196681
	− 2.71170	− 0.026044	2.141190	5.438882	− 3.315185	− 11.082296	− 1.925179	− 7.403175	− 2.650197	− 0.064719	− 2.327481
	1.025211	0.084502	3.609852	11.264976	− 0.563585	1.051008	3.364952	− 0.039077	1.438832	− 0.502388	0.244119
	− 5.115017	− 1.617317	_− 0.544702	− 11.532799	− 1.514084	− 2.345942	− 1.575634	− 1.516767	− 2.529654	− 2.711580	− 1.820048
	1.856833	1.000783	3.106941	_0.483910	− 4.384302	0.132833	− 0.522259	− 0.845249	0.630193	3.169898	1.703590
	− 0.699439	0.398309	− 0.871634	− 0.562051	− 2.026843	− 2.291823	1.122091	− 2.227168	− 0.001197	0.236927	0.222279
	− 0.684422	− 0.227036	0.442206	0.159065	− 0.187215	4.077606	− 1.212950	0.395407	− 3.971782	− 1.874380	− 0.424155
	2.575882	0.873076	0.753464	− 0.381804	0.209684	1.106739	0.324285	− 3.294926	0.910453	4.455526	− 0.210606
	− 2.792995	0.973368	− 0.980339	_− 6.199725	− 0.813543	− 0.179206	0.861033	− 2.176371	0.058426	0.151638	− 0.634437
	0.055632	− 1.110344	0.016177	_− 3.054829	− 1.224742	− 0.702527	− 1.879655	0.768483	1.226748	− 1.153990	− 0.572318
	− 7.453501	− 2.425148	− 1.6/3242	0.666105	− 1.403058	− 0.656834	− 5.761195	− 2.523870	− 2.172658	− 2.463700	− 1.600084
	− 0.831939	1.905886	4.208505	0.729582	− 2.376741	− 4.753372	1.532718	0.246998	− 0.456729	2.346060	0.101476
	− 0.218895	− 1.282917	− 2.438997	− 4.988396	− 0.695354	− 8.302355	6.776245	5.263532	11.788553	− 0.695016	0.581765

Table 6 continued

From node	50	51	52	53	54	55	56
To nodes 57–71	0.585169	2.200735	1.003896	0.983211	− 2.686751	− 1.874919	− 3.639469
	− 1.266654	2.539963	0.951732	− 0.597016	− 0.761802	1.694966	1.303102
	− 2.718170	− 1.478810	0.840517	0.267168	− 0.009130	1.202395	− 0.759940
	3.735235	− 0.405097	1.383265	− 3.315771	− 0.947991	− 0.159326	4.719949
	− 1.006926	− 0.263174	− 1.802892	0.282114	4.875757	− 1.482199	0.843602
	− 2.740616	1.717481	− 1.173034	− 2.203490	4.236280	− 4.480697	0.324572
	− 1.097945	4.425057	0.621333	− 1.083926	− 0.337695	2.219592	0.575963
	− 4.263931	0.497684	− 1.102987	− 0.361218	− 0.863358	− 3.380723	0.620700
	− 2.325255	0.140052	− 1.313278	− 2.870618	− 0.266015	− 1.181687	− 0.409093
	− 0.919146	0.963642	− 0.325819	− 0.690391	− 0.865093	− 2.611176	− 0.630341
	− 2.544491	− 0.777000	− 1.550774	− 1.202771	− 1.090545	− 5.059728	2.999128
	0.057299	− 0.542813	0.310875	0.387294	− 1.048504	0.296622	0.594172
	− 0.943888	− 0.270077	− 1.603716	4.321634	1.173412	4.219301	8.374449
	8.079837	0.632799	1.481626	− 6.662017	0.733916	4.093148	0.579841
	5.055160	− 0.450023	− 0.537895	− 10.314010	− 1.793091	− 0.923884	− 4.484211

Table 7 The weight values for connections between the second hidden layer and the output node

From node	57	58	59	60	61	62	63	64
To node 72	− 0.846016	− 0.984912	− 1.469878	4.183980	− 1.768924	− 2.352588	− 6.605018	− 1.199227
From node	65	66	67	68	69	70	71	
To node 72	− 1.513517	− 0.867614	− 2.843237	− 2.055631	1.230391	− 1.061599	− 1.769187	

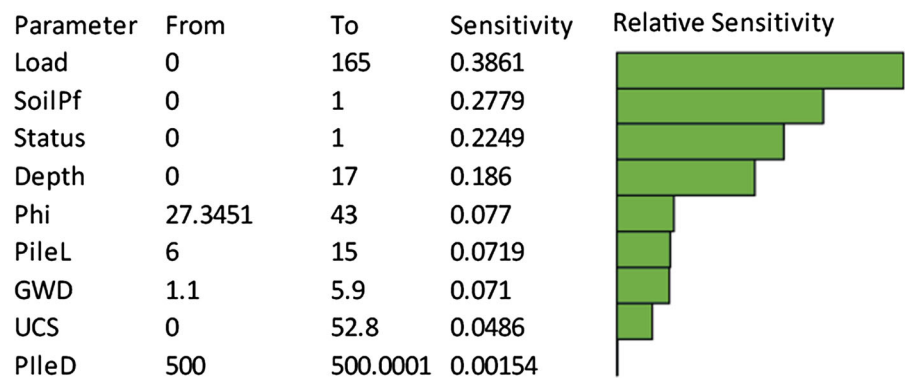

Fig. 8 Sensitivity analysis of the input parameters

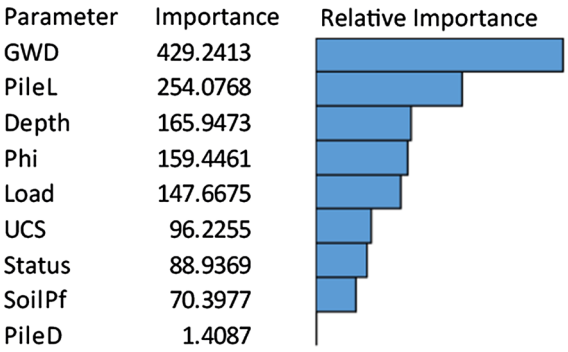

Fig. 9 The input importance and relative importance

the same as that measured in the field. In both situations, the pile did not experience the 1% ratio of downward movement to fully mobilize the friction resistance, the pile, in fact, moved only 0.51% of its diameter. Figure 11 shows the displacement predicted by the model along with the displacement from the field at each load. It is obvious that the predicted displacement values at each load almost coincide with the actual displacement.

In Fig. 11, the model predicted a maximum displacement of 2.58 mm while the actual displacement was 2.77 mm, note that the difference between the two is less than 0.19. In both situations, the pile moved about 0.55% of its diameter. Although the model slightly underestimates the displacement, the difference is not significant from a practical point of view. Figure 10 shows the displacement predicted by the model along with the displacement from the field at each load. It is obvious that the predicted displacement values at some loads were overestimated or underestimated. In either case, the difference was almost negligible.

In Fig. 12, the model predicted a maximum displacement of 1.34 mm while the actual displacement was 1.22 mm. Again, the difference between the two is less than 0.12 mm and the pile in the model moved about 0.27% of its diameter. Figure 12, also, shows the displacement predicted by the model along with the displacement from the field at each load. The predicted displacement values were slightly underestimated in the first two cycles and slightly overestimated in the last two cycles. In either case, the difference was not substantial but can be overcome when the sample data is increased to cover more cases.

9.2 Displacement Regression Graphs

The predicted and actual displacement values were plotted against each other to illustrate the relationship between them as shown in Figs. 13, 14 and 15. To

Table 8 Soil profiles for the three pile tests used in the query files to verify the ANN approach

Test #	BH and its properties			
Test 1	Depth (M)	Ø (°)		UCT Kg/cm^2
	0.0	31.4	Silty Sand	0
	0.5	31.4		0
	1.0	34.1		0
	1.5	34.1	G.W.T	0
	2.0	29.9		0
	2.5	29.9		0
	3.0	35		13.5
	3.5	35	Calcarnite	13.5
	4.0	37		17.2
	4.5	37		17.2
	5.0	38		19.1
		38		19.1
	5.5	42	Mudstone	43.1
	6.0			
Test 2	Depth (M)	Ø (°)		UCT Kg/cm^2
	0.0	32.1		0
	0.5	33		0
	1.0	33		0
	1.5	33	G.W.T	0
	2.0	33	Silty Sand	0
	2.5	31		0
	3.0	31		0
	3.5	31		0
	4.0	34		12.1
	4.5	34		12.1
	5.0	36		15.3
		36		15.3
	6.0	38	Calcarnite	19.3
	7.0			
Test 3	Depth (M)	Ø (°)		UCT Kg/cm^2
	0.0	34.1		0
	1.0	34.1		0
	1.5	27.3		0
	2.0	27.3		0
	2.0	27.3		0
	2.5	29.9	G.W.T	0
	3.0	29.9		0
	3.5	38.4		0
	4.0	38.4		0
	4.5	33.9	Silty Sand	0
	5.5	36.1		0
		36.1		0
	7.0	38.4		0
	8.5	38.4		0

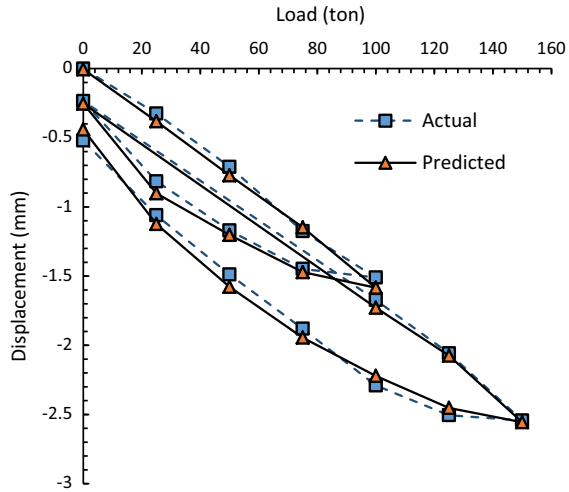

Fig. 10 Conventional load–displacement curve, showing both the predicted and the actual results for query file 1

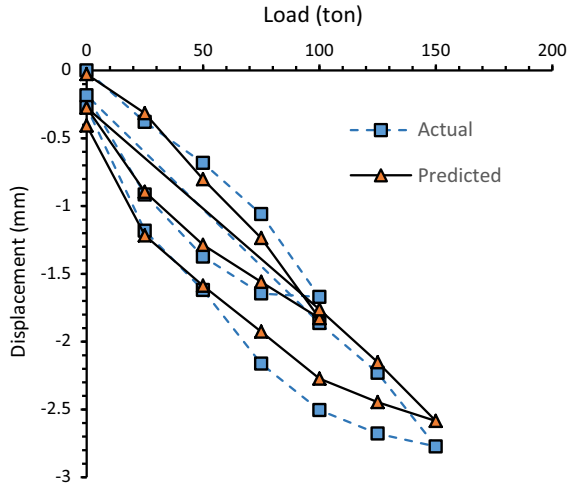

Fig. 11 Conventional load–displacement curve, showing both the predicted and the actual results for query file 2

demonstrate how close, the values to the diagonal line, the best-fit line along with its equation and R^2 are also shown in the same figures. Table 9 shows the equation of the lines as well as the line R^2 values. As shown in the figures and the table, and considering the entire range of data, the accuracy of the model is above 90%. Moreover, all R^2 values of the tests were high which indicate that all points are close to the diagonal line.

The accuracy of the three runs is measured by calculating the average error between the actual and

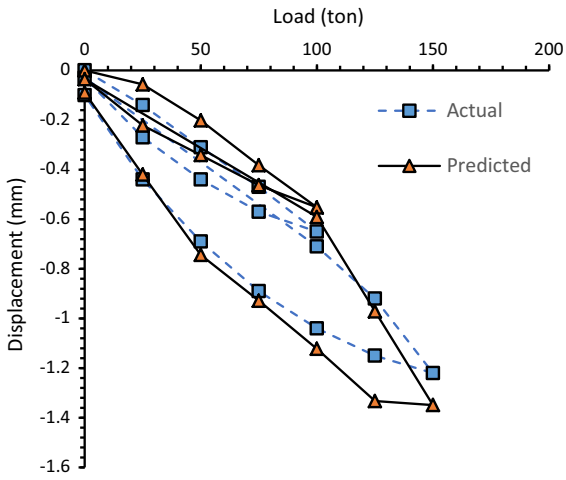

Fig. 12 Conventional load–displacement curve, showing both the predicted and the actual values for query file 3

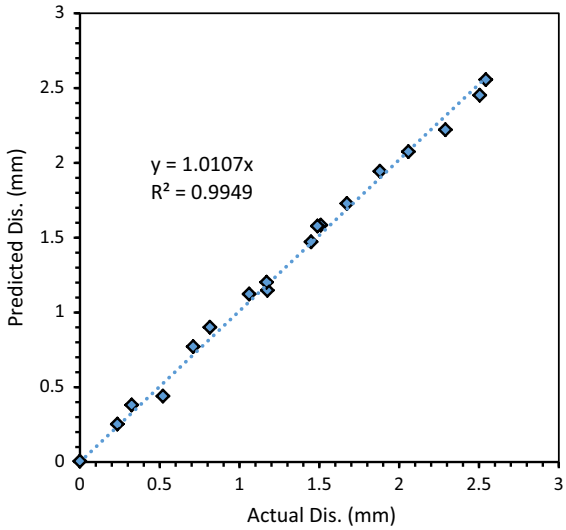

Fig. 13 Predicted versus actual displacement into one–one graph for query file 1

the predicted displacement values. Figure 16 shows the average percentage error at each loading point starting from 0 to 150 tons. In the graph, the positive error shows overestimation while the negative one shows underestimation. As shown in the figure, the maximum average error was − 20% which occurred at only one point at the beginning of the loading curve. At higher loads, the average error decreased to nearly 1%. In summary, the average error of all the data points was approximately − 1%.

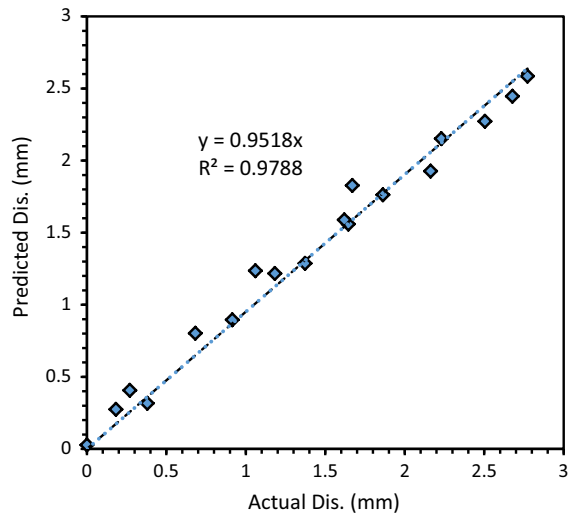

Fig. 14 Predicted versus actual displacement into one–one graph for query file 2

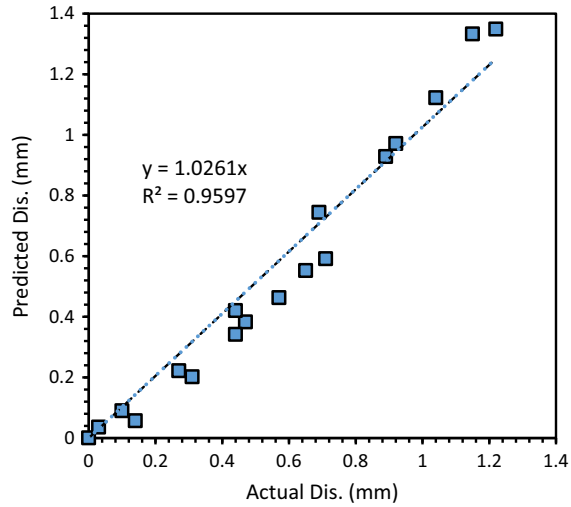

Fig. 15 Predicted versus actual displacement into one–one graph for query file 3

The proposed model shows that the load–displacement curves of a static pile load test, in the area of interest and a pile diameter of 500 mm, can be predicted with a minimum accuracy of 80%.

10 Conclusion

This paper introduced a new approach to predict the entire static load tests curves using a backpropagation

Table 9 Summary of the tests results, equations of the lines and R^2

Test Number	Equation	R^2
1	$y = 1.0107x$	0.9949
2	$y = 0.9518x$	0.9788
3	$y = 1.0261x$	0.9597

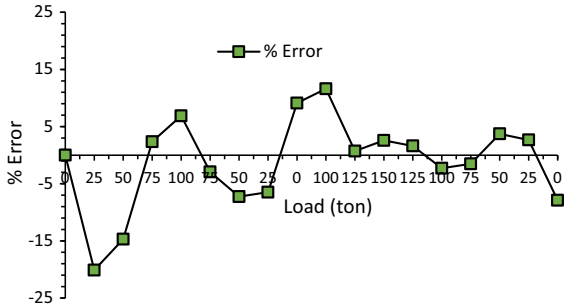

Fig. 16 The model percentage errors

neural network model. The model was trained using data collected from three cities located in the UAE. The model was fed with the geotechnical data such as friction angle, unconfined compressive strength and soil type with depth, the groundwater table elevation, a fixed pile's diameter of 500 mm, pile's length, and load–displacement curves to train the model. However, with this approach, more data having variant geological formations and additional pile configurations should be incorporated in the training to generalize the model.

Three independent pile tests were used to test the model. Two loading and two unloading curves were successfully obtained by the proposed model. The actual data were compared with the predicted data and regression analysis showed that the model predicted the displacement with R^2 average of 0.9778. By including all the necessary data that affect the CFA pile's behavior, it was possible to simulate the entire Static Load Test with an average error of about 1%. The sensitivity analysis showed that all the chosen parameters were relevant and played an important role in the model performance.

This approach with this amount of data from UAE showed great potential in cutting the costs associated with multiple static load tests. Moreover, this approach provides an excellent tool in the hands of designers ahead of any site work. It increases their ability to predict the pile performance and modify their design ahead of conducting the actual field test.

Acknowledgements The authors would like to extend their gratitude to the office of scholarship and sponsorship programs at Abu Dhabi University for their financial support of this project, Grant No. 19300304.

References

Abu Kiefa MA (1998) General regression neural networks for driven piles in cohesionless soils. J Geotech Geoenviron Eng ASCE 124(12):1177–1185

Alzo'ubi AK, Ati M, Ibrahim F (2015) Smart framework for predicting drilled shaft capacity based on data mining techniques and GIS data. In: Manzanal D, Sfriso AO (eds) From fundamentals to applications in geotechnics, The Pan American conference on soil mechanics and geotechnical engineering, 15th PCSMGE/8th SCRM/6th IS-BA 2015, 15–18 November, 1909–1915

ASTM D1586-11 (2011) Standard test method for standard penetration test (SPT) and split-barrel sampling of soils. ASTM International, West Conshohocken. https://doi.org/10.1520/d1586-11, www.astm.org

Benali A, Ammar N (2011) Prediction of the pile capacity in purely coherent soils using the approach of the artificial neural networks. In: International seminar, innovation and valorization in civil engineering and construction materials, No.: 5O-239, University of sciences and technology, Algiers, Algeria

BS 8004:2015. BSI Standards Publication Code of practice for foundations BS 8004:2015 BRITISH STANDARD

Coduto DP (2001) Foundation design, principles and practices, 2nd edn. Prentice Hall, Upper Saddle River

Crowther CL (1988) Load testing of deep foundations. Wiley, New York

Das B (2016) Principles of foundation engineering, 8th edn. Cengage Learning, Boston

Fookes PG, Knill JL (1969) The application of engineering geology in the regional development of northern and central Iran. Eng Geol 3:81–120

Geman E et al (1992) Neural networks and the bias/variance dilemma. Neural Comput 4:1–58

Goh ATC (1995) Empirical design in geotechnics using neural networks. Geotechnique 45:709–714

Goh ATC (1996) Pile driving records reanalyzed using neural networks. J Geotech Geoenviron Eng ASCE 122(6):492–495

Han J, Kamber M (2012) Data mining, concepts and techniques, 3rd edn. Morgan Kaufman Publishers, Burlington

Hatanaka M, Uchida A (1996) Empirical correlation between penetration and resistance and internal friction angle of sandy soils. Soils Found 36(4):1–10

Haykin S (1999) Neural networks, a comprehensive foundation. Macmillan College Publishing Co., New York

Lee IM, Lee JH (1996) Prediction of pile bearing capacity using artificial neural networks. Comput Geotech 18(3):189–200

Liao SSC, Whitman RV (1985) Overburden correction factors for SPT in sand. J Geotech Eng ASCE 112(3):373–377

Liu et al (2008) Optimized approximation algorithm in neural networks without overfitting. IEEE Trans Neural Netw 19(6):983–995

Maizir H, Kassim K (2013) Neural network application in prediction of axial bearing capacity of driven piles. In: Proceedings of the international multi conference of engineers and computer scientists, Hong Kong

Meyerhof GG (1965) Shallow foundations. J Soil Mech Found Div ASCE 91(2):21–31

Neural Planner Software (2016) EasyNN plus. www.easyNN.com, USA

Prechelt L (2012) Early stopping—but when? In: Montavon G, Orr GB, Müller K-R (eds) Neural networks: tricks of the trade. Springer, Berlin, pp 53–67

Shahin MA, Jaska MB, Maier HR (2001) Artificial neural network applications in geotechnical engineering. Aust Geomech 36:49–62

Skempton AW (1986) Standard penetration test procedures and the effects in sands and overburden pressure, relative density, particle size, aging and over consolidation. Geotechnique 36(3):425–447

Tarawneh B (2013) Pipe pile setup: database and prediction model using artificial neural network. Soils Found 53(4):607–615

Terzaghi K (1943) Theoretical soil mechanics. Wiley, New York

The code handbook: Abu Dhabi International Building Codes, 2013. Department of Municipal Affairs, Abu Dhabi

Tomlinson M, Woodward John (2014) Pile design and construction, 6th edn. CRC Press, Boca Raton